

# Nuclear modification factor within a dynamical approach to the complex entropic index

R. Baptista<sup>1</sup>, L. G. Rocha<sup>1</sup>, J. M. C. Pareja<sup>1</sup>, T. Bhattacharyya<sup>2</sup>, A. Deppman<sup>1</sup>,  
E. Megías<sup>3,\*</sup>, M. Rybczyński<sup>2</sup>, G. Wilk<sup>4</sup>, Z. Włodarczyk<sup>2</sup>

1- Instituto de Física - Universidade de São Paulo, Rua do Matão 1371, São Paulo 05508-090, Brazil

2- Institute of Physics Jan Kochanowski University, 25-406 Kielce, Poland

3- Departamento de Física Atómica, Molecular y Nuclear and Instituto Carlos I de Física Teórica y Computacional, Universidad de Granada, Avenida de Fuente Nueva s/n, 18071 Granada, Spain

4- National Centre For Nuclear Research, Pasteura 7, Warsaw 02-093, Poland

---

## Abstract

This work introduces a novel approach to the nuclear deformation factor  $R_{AA}$ , grounded in the dynamical effects of the Quark-Gluon Plasma on parton momentum. The approach uses the Blast-Wave method combined with Tsallis Statistics, within the Copper-Frye freeze-out framework and, by profiting from appropriate simplifications, it gives analytical expressions that describe the observed  $R_{AA}$  for two sets of independent measurements at  $\sqrt{s} = 2.76$  TeV and  $\sqrt{s} = 5.02$  TeV. A nonlinear dynamical equation describes the dynamics and leads to log-periodic oscillations. With the analytical solutions for that equation, it is possible to link the dynamical approach with the complex- $q$  formalism, which was proposed to describe the log-oscillations observed in experimental data.

---

## 1. Introduction

One of the most accessible observables in high-energy collisions is the transverse momentum distribution. These distributions are relatively straightforward to measure and offer valuable insight into the underlying collision dynamics. Experimental data consistently show that the overall shape of these distributions is well described by Tsallis statistics, where the probability distribution is proportional to the  $q$ -exponential function:

$$g(x) \propto e_q(-x) = [1 + (q-1)x]^{\frac{-1}{q-1}}, \quad (1)$$

with  $q > 1$  denoting the entropic index and  $x > 1/(1-q)$ .

Detailed analyses reveal that, beyond the nonextensive character captured by the  $q$ -exponential form, transverse momentum spectra also exhibit log-periodic oscillations. These oscillations can be understood by allowing the entropic index  $q$  to take on complex values, which corresponds, in the thermodynamic interpretation, to a complex specific heat for the system formed during the collision [1, 2]. In this context, the

generalized  $q$ -exponential function takes the form:

$$g(E) \cong \left[1 + \frac{E}{nT}\right]^{-m_0} \left\{ w_0 + w_1 \cos \left[ \frac{2\pi}{\ln(1+\alpha)} \ln \left(1 + \frac{E}{nT}\right) \right] \right\}, \quad (2)$$

where  $m_0 = -\ln(1 - \alpha n)/\ln(1 + \alpha)$ , which approaches  $m_0 = n = \frac{1}{q-1}$  in the limit  $\alpha \rightarrow 0$ . The physical interpretation of the complex values for the parameter  $q$  is linked to complex specific heat [3] and temperature oscillations associated with sound waves in the hadronic matter [4, 5].

This work presents a novel approach to calculating the dynamical effects of the expanding medium on the particle momentum distribution. Unifying plasma expansion and hadronisation, this work proposes a simple and effective way to address the dynamics of the quark-gluon plasma. The nuclear modification factor and logarithmic oscillations appear as manifestations of the same dynamical effects. Therefore, the present work contributes to the ongoing efforts to interpret the complex-valued entropic index  $q$  by exploring the potential connections with the dynamical aspects of the system formed in high-energy collisions. This novel approach preserves consistency with the nonlinear dynamics resulting from non-local correlations in the medium, while extending the scope of nonextensive methods to dynamical processes in the quark-gluon plasma.

Transverse momentum distributions in nucleus–nucleus collisions differ markedly from those in proton–proton collisions, with a strong dependence on collision centrality. In nucleus–nucleus interactions, the system undergoes a centrality-dependent expansion following the formation of the quark–gluon plasma (QGP). During this evolution, numerous partons are produced while the system’s temperature decreases. Eventually, the QGP freezes out, leading to the production of a large number of hadrons. This entire process can be broadly divided into three stages: initial particle production, QGP expansion, and freeze-out.

This work analyses the transverse momentum spectra in both nucleus–nucleus and proton–proton collisions, focusing on their differences as quantified by the nuclear modification factor  $R_{AA}$ , defined as

$$R_{AA}(p_T) = \frac{1}{N_{\text{coll}}(\epsilon)} \frac{dN^{AA}/dp_T dy}{dN^{pp}/dp_T dy}, \quad (3)$$

where  $dN^{AA}/dp_T dy$  and  $dN^{pp}/dp_T dy$  are the differential yields in nucleus–nucleus and proton–proton collisions, respectively, and  $N_{\text{coll}}(\epsilon)$  is the number of binary nucleon–nucleon collisions for a given centrality  $\epsilon$ . Our analysis explores the microscopic origin of the complex  $q$  parameter and its implications for the dynamical behaviour of parton momentum distributions.

The main objective is to compute the nuclear modification factor by analysing each stage of the reaction individually. To this end, we adopt the following assumptions:

1. Partons produced in the initial stage follow the same transverse momentum distribution as in proton–proton ( $pp$ ) collisions.
2. The system’s expansion is described by the Blast-Wave model, assuming axial symmetry.

3. The in-medium parton dynamics is governed by the non-linear Plastino–Plastino Equation (PPE).
4. The freeze-out surface has cylindrical geometry and, in the region responsible for most observed particles, exhibits axial symmetry.

## 2. Theoretical Development

In the initial stage of the collision, particles are produced via interactions among a subset of partons from the colliding nuclei, with the number of such binary parton-parton collisions denoted by  $N_{\text{coll}}(\epsilon)$ , which depends on the collision centrality  $\epsilon$  [6, 7]. The transverse momentum distribution of the partons created at this stage is represented by  $f(p_T)$ .

As the system evolves, collective motion becomes dominant. The produced partons interact strongly, giving rise to a complex, non-linear medium characterized by non-local correlations [8, 9, 10]. This expansion stage plays a crucial role in shaping the observed particle distributions.

Eventually, the system hadronizes and undergoes freeze-out, leading to the emission of a large number of hadrons. This process is typically described using the Cooper–Frye formalism, which models particle production through the momentum flux across a three-dimensional hypersurface embedded in four-dimensional space-time [11].

### 2.1. Cooper–Frye mechanism in the Blast-Wave picture

The Cooper–Frye approach assumes that freeze-out occurs when the expanding QGP reaches a three-dimensional surface  $\Sigma(x_0, x_1, x_2, x_3)$  in relativistic spacetime. The Lorentz-invariant particle yield is given by

$$E \frac{dN}{d^3p} = \frac{1}{(2\pi)^3} \int dN^\mu p_\mu f^{AA}(p), \quad (4)$$

where  $dN^\mu$  is the normal vector to the freeze-out hypersurface, and  $f^{AA}(p)$  is the particle momentum distribution.

For a longitudinally boost-invariant system, the freeze-out surface can be written as

$$\Sigma_\mu = (\tau(x,y) \cosh \eta, x, y, \tau(x,y) \sinh \eta), \quad (5)$$

where  $\tau(x,y)$  is the proper time, and  $\eta$  is the spacetime rapidity. The free parameters in this parametrisation are  $x$ ,  $y$ , and  $\eta$ . The corresponding normal vector is

$$dN_\mu = \left( \cosh \eta, -\frac{\partial \tau}{\partial x}, -\frac{\partial \tau}{\partial y}, -\sinh \eta \right) \tau(x,y) dx dy d\eta. \quad (6)$$

The four-momentum of a particle is given by

$$p^\mu = (m_T \cosh \eta', p_x, p_y, m_T \sinh \eta'), \quad (7)$$

where  $\eta'$  is the particle rapidity, and  $m_T = \sqrt{p_x^2 + p_y^2 + m^2}$  is the transverse mass. The scalar product between  $p^\mu$  and  $dN_\mu$  becomes

$$p^\mu \cdot dN_\mu = \left( m_T \cosh(\eta' - \eta) - p_x \frac{\partial \tau}{\partial x} - p_y \frac{\partial \tau}{\partial y} \right) \tau dx dy d\eta. \quad (8)$$

The momentum distribution in Eq. (4) is generally expressed as a function of the Lorentz-invariant quantity  $p^\mu u_\mu$ , where the fluid four-velocity is

$$u_\mu = \gamma_v (\cosh \eta, -v_x, -v_y, -\sinh \eta), \quad (9)$$

and  $\gamma_v = (1 - v^2)^{-1/2}$  is the Lorentz factor associated with the transverse flow velocity.

When the fluid crosses the freeze-out surface, it hadronizes, and the observed particle spectrum is obtained by integrating over all fluid elements:

$$E \frac{dN}{d^3 p} = \frac{1}{(2\pi)^3} \int dx dy d\eta \tau(x, y) \left( m_T \cosh(\eta' - \eta) - p_x \frac{\partial \tau}{\partial x} - p_y \frac{\partial \tau}{\partial y} \right) f(p^\mu u_\mu). \quad (10)$$

In the blast-wave approach, several simplifying assumptions are adopted. First, the fluid expansion is assumed to be axially symmetric [12], allowing the substitution  $dx, dy \rightarrow 2\pi r_T dr_T$ , where  $r_T$  is the radial distance from the symmetry axis. Consequently, the freeze-out proper time becomes a function of the radial coordinate only:  $\tau(x, y) = \tau(r_T)$ .

Although the proper freeze-out time generally depends on the radial position due to the combined radial and longitudinal expansion of the fluid, in the version of the Blast-Wave model used here, most particles are emitted from a narrow cylindrical shell along the longitudinal direction. This behavior arises from the explosive nature of the system, which imparts momentum to the entire fluid almost instantaneously, resulting in an approximately uniform longitudinal velocity. As a consequence, the freeze-out time can be considered nearly independent of  $r_T$ , so that  $\partial \tau / \partial x = 0$  and  $\partial \tau / \partial y = 0$ , implying  $\tau(r_T) = \tau = \text{const}$ . Under this approximation, the QGP freeze-out is considered *quasi-instantaneous*.

Additionally, we assume that the central region of the fluid moves longitudinally with rapidity confined to a narrow interval  $\Delta \eta$  around  $\eta = 0$ . Since most of the detected particles are produced in this region, the integration over the fluid rapidity simplifies the expression for the invariant yield, which becomes:

$$E \frac{dN}{d^3 p} = \frac{r_T^2 \tau}{8\pi^2} \Delta \eta m_T \cosh \eta' f(p^\mu u_\mu). \quad (11)$$

## 2.2. Dynamics of partons in the medium

The partons, while moving through the medium, interact and deposit energy into that medium, and they can reach a quasi-exponential stationary state [13] as a result of anomalous diffusion. The anomalous diffusion of parton momentum is described by the Plastino–Plastino Equation (PPE), given by [14]

$$\frac{\partial f}{\partial t} - \frac{\partial}{\partial p_i} \left[ A(p_i) f + \frac{\partial}{\partial p_i} (D f^{2-q}) \right] = 0, \quad (12)$$

where  $A$  and  $D$  are the transport coefficients associated, respectively, with drag and (isotropic) diffusion.

As the PPE is derived from the Fokker–Planck Equation (FPE) by considering dynamics in fractal spaces, it remains essentially non-relativistic. Relativistic generalisations of the FPE have been proposed [15] and are widely used in studies of electromagnetic plasmas. The main difference compared to the PPE is that the time differential operator must be multiplied by the particle energy  $E$ . However, this seemingly simple modification prevents the derivation of analytical solutions. In this work, we adopt the non-relativistic version, acknowledging that predictions for high-momentum partons ( $p \gg m$ ) may underestimate relativistic effects. As will become clear below, such corrections can, in some cases, be effectively absorbed into other parameters of the model.

The PPE has been employed to describe the dynamics of partons in the quark–gluon plasma (QGP). This approach is motivated by the fact that the stationary solutions of the PPE exhibit the  $q$ -exponential form observed in experimental data. While the PPE is valid for a stationary medium, the QGP formed in nucleus–nucleus collisions undergoes rapid expansion as partons propagate through it. Our objective is to investigate how the expanding medium influences the stationary solutions of the PPE.

The PPE calculates dynamical effects in the local fluid rest frame, thus the relevant momentum for the dynamics is<sup>1</sup>

$$\bar{p}_T^o = L_u[p_T^o], \quad (13)$$

where  $p_T^o$  is the parton’s average transverse momentum at the moment of creation. The main effect of the dynamical processes in the medium is the modification of the parton’s momentum, given by

$$\bar{p}_T = \bar{p}_T^o \exp(-A\tau), \quad (14)$$

where  $\tau$  is the time elapsed between QGP formation and freeze-out. The parton momentum in the CM frame is obtained by the inverse Lorentz transformation:

$$p_T = L_{-u}[\bar{p}_T]. \quad (15)$$

In the equations above,  $L_{\pm u}$  represents the Lorentz transformation of the CM momentum to (+) and from (−) the fluid frame.

For convenience, the Lorentz transformations are considered separately. The transformation of the space-like components of the momentum is

$$L_u(\vec{p}) = \gamma_v (\vec{p} - \vec{v}E), \quad (16)$$

and the transformation of the time-like component is

$$L_u(E) = \gamma_v (E - \vec{v} \cdot \vec{p}), \quad (17)$$

where  $E = \sqrt{\vec{p}^2 + m^2}$  and  $u^\mu = \gamma_v(1, \vec{v})$  is the local fluid velocity.

---

<sup>1</sup>In this subsection and in the rest of the manuscript, we omit arrows for 3-vectors. It should be understood that  $p \equiv \vec{p}$  and  $v \equiv \vec{v}$ , unless stated otherwise.

The separation between space-like and time-like components is convenient since the dynamical effects are associated solely with the space-like components. To recover the transverse momentum before the drift effects, the following relation is used:<sup>2</sup>

$$\vec{p}_T^o = L_{-u} [\exp(A\tau) L_u [\vec{p}_T]] , \quad (18)$$

and the time-like component is calculated to maintain mass invariance,

$$E^o = \sqrt{\vec{p}_T^{o,2} + m^2} , \quad (19)$$

representing the parton energy before drift effects. With  $\vec{p}_T^o$  and  $E^o$ , one forms the full four-momentum of the created parton with mass  $m$ .

It is assumed that the momentum distribution at the moment of parton creation has the same functional form for  $pp$  and  $AA$  collisions, and is described by [16]

$$E \frac{dN}{d^3p} = \frac{gVm_T \cosh \eta'}{(2\pi)^3} f(p_T) , \quad (20)$$

where

$$f(p_T) = N \left[ 1 + (q-1) \frac{m_T \cosh \eta' - \mu}{T} \right]^{-\frac{q}{q-1}} , \quad (21)$$

with  $q = 1.16$ ,  $T$  being the temperature,  $g$  the degeneracy factor,  $N$  the particle multiplicity, and  $V$  the system volume. Note that from Eqs.(20) and(21), the distribution satisfies  $dN/d^3p \propto N/E$ .

In  $AA$  collisions, this distribution is deformed due to interactions with the expanding medium. For a given observed momentum  $p_T$ , the modified distribution  $f^{AA}(p_T)$  becomes

$$f^{AA}(p_T) = f(p_T^o) = f(L_{-u} [\exp(A\tau), L_u [p_T]]) , \quad (22)$$

where Eq. (18) has been used.

### 2.3. Particle multiplicity and nuclear modification factor

Multiparticle production is inherently a non-extensive process. One of its key consequences is the non-linear relationship between the total collision energy and the produced particle multiplicity. This relationship can be expressed as

$$N \propto E^{1-d} , \quad (23)$$

where  $d$  is the fractal dimension of the QGP, expected to be  $d = 0.69$  [17]. From this scaling, the ratio of multiplicity to energy follows

$$\frac{N}{E} \propto E^{-d} . \quad (24)$$

---

<sup>2</sup>By considering the Lorentz transformation of the energy, the expression relating the initial energy  $E_o$  with the final energy  $E$  of the parton turns out to be  $E_o = L_{-u} \left( \sqrt{m^2 + (L_u(E)^2 - m^2) \exp(2A\tau)} \right)$ . It is easy to check that this expression agrees with the simpler formula written in Eq. (18).

This behaviour indicates that the system formed in high-energy collisions is non-extensive, since the total energy does not scale linearly with the number of particles. Importantly, the total energy depends on the collision centrality, which is characterised by the fraction of nucleons participating in the overlap region of the colliding nuclei. It is therefore reasonable to assume that the effective energy available for particle production scales as

$$E \propto 1 - \epsilon, \quad (25)$$

where  $\epsilon$  parametrises the nuclear eccentricity.

Taking this into account, the nuclear modification factor can be expressed as

$$R_{AA} = K(1 - \epsilon)^{-d} \frac{V_{AA}}{V_{pp}} \frac{f(L_{-u}[L_u[p], \exp(A\tau)])}{f_{\Delta p_l}(p_T)}, \quad (26)$$

where  $K$  is a constant and  $V_{AA}$ ,  $V_{pp}$  are the freeze-out volumes in  $AA$  and  $pp$  collisions, respectively. Since  $K$ ,  $V_{AA}$ , and  $V_{pp}$  are not independently known, it is convenient to group them into a single parameter:

$$R_{AA}^0 = K \frac{V_{AA}}{V_{pp}}. \quad (27)$$

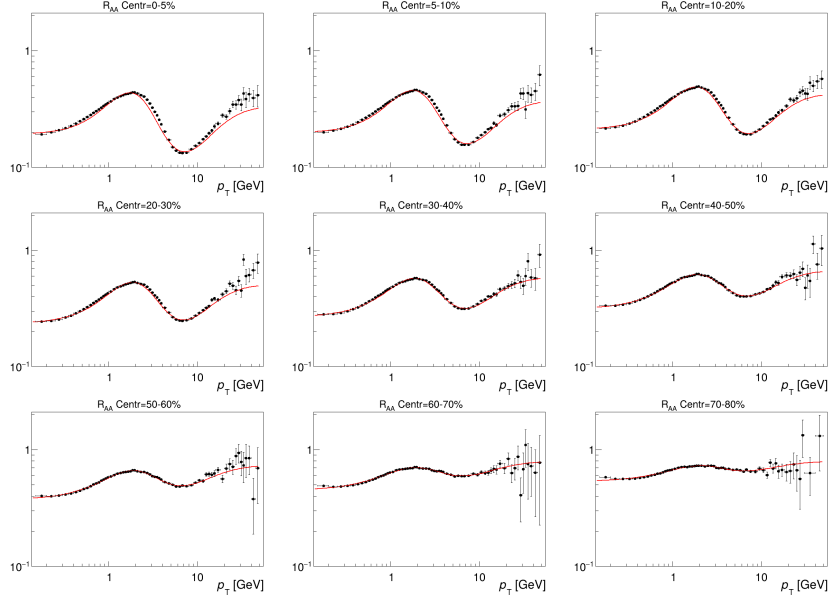


Figure 1: ALICE experimental data (black circles) for the  $R_{AA}$  of charged particle production in PbPb collisions at  $\sqrt{s_{NN}} = 2.76$  TeV [18], compared with theoretical results (full line). The plots are for centrality bins 0 – 5%, 5 – 10%, 10 – 20%, 20 – 30%, 30 – 40%, 40 – 50%, 50 – 60% and 70 – 80% respectively.

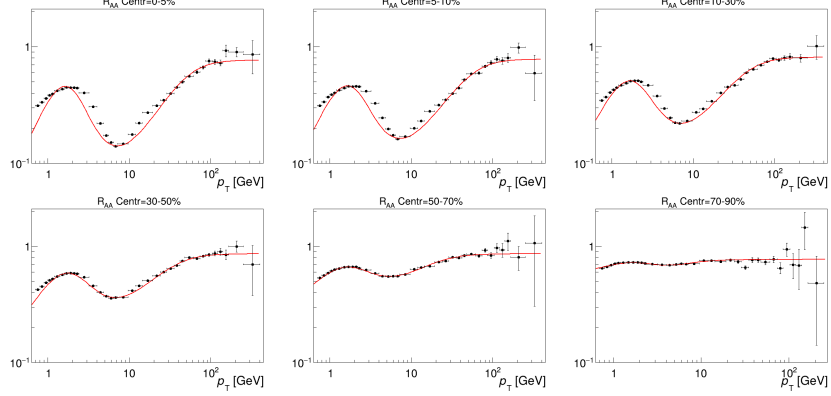


Figure 2: CMS experimental data (black circles) for  $R_{AA}$  of charged particle production in PbPb collisions at  $\sqrt{s_{NN}} = 5.02$  TeV [19] compared with theoretical results (full line). The plots are for centrality bins 0 – 5%, 5 – 10%, 10 – 30%, 30 – 50%, 50 – 70% and 70 – 90% respectively.

#### 2.4. Dynamical effects on the momentum

Let us first consider only the drift term of the PPE. The behaviour of the drift coefficient,  $A(p)$ , as it relates to the parton's momentum in the fluid frame, is crucial for accurately describing the high transverse momentum sector of  $R_{AA}$ . While a detailed calculation of  $A(p)$  is complex [8], a phenomenological approach is sufficient for this study. The momentum dependence can be modelled by considering that the running coupling, which quantifies the strength of the partons' interaction with the medium, follows a  $q$ -exponential function with  $q = 1.16$  [20]. Therefore, the momentum-dependent drift coefficient is given by:

$$A(p_T) = A_o \exp_q [-\bar{m}_T/T_D] , \quad (28)$$

where  $T_D$  is associated with the energy scale of the dynamical effects.

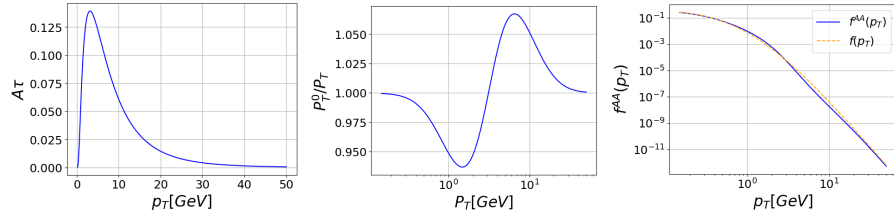


Figure 3: (Left) The drag coefficient as a function of the transverse momentum. (Centre) The oscillation of the initial momentum  $p_T^o$  of the parton as a function of the observed momentum  $p_T$ . (Right) The AA momentum distribution after dynamical effects,  $f^{AA}$ , as a function of the observed transverse momentum (solid line), compared to the  $pp$  transverse momentum distribution for  $pp$  collision,  $f$ .

The diffusion effects, governed by the stochastic term in the PPE, were also evaluated (see Supplementary Material for additional information). However, the analysis shows that the diffusion effects in the nuclear modification factor are negligible.



### 3. Results and discussion

The formalism developed above was applied to generate theoretical curves fitted to experimental data on charged particle production in PbPb collisions at  $\sqrt{s_{NN}} = 2.76$  TeV and  $\sqrt{s_{NN}} = 5.02$  TeV. The analysis focuses on the nuclear modification factor  $R_{AA}$  as a function of the parton transverse momentum, measured for various collision centralities [18, 19]. The results are presented in Figs. 1 and 2 for the respective energies and centralities. For taking into account the effects of fluid expansion, the temperature of the AA distribution,  $T_{kin}$ , is allowed to differ from that for the  $pp$  collisions.

A fair agreement is observed between the theoretical predictions and the experimental data, indicating that the dynamical effects captured by the model can reproduce the oscillatory behaviour of the  $R_{AA}$ . Discrepancies appear in both the low- and high- $p_T$  regions (up to 50% centrality), likely due to relativistic effects not included in the current formulation. It is worth noting that, after the Lorentz transformation, both low and high momenta in the centre-of-mass frame correspond to relatively high momenta in the local fluid rest frame.

A central aspect of the observed agreement between data and calculations is the inclusion of the nonextensive aspects of the multiparticle production through Eq. (24), which determine the overall intensity of the nuclear deformation. This represents strong evidence of the nonextensivity in the particle production. The fact that it is reproduced by employing the fractal exponent  $d$  aligns with recent connections between Tsallis Statistics and fractal structures in QCD [20].

The free parameters used in the fits are  $u$ ,  $D_0 = A_0\tau$  (where  $\tau$  is the freeze-out time),  $R_{AA}^0$ ,  $T_{Kin}$  (the temperature derived from the AA spectra), and  $T_D$  (the temperature associated with the drag function  $A(p_T)$ ). The parameter  $T_{pp}$  in the denominator of  $R_{AA}$  is fixed from the description of  $pp$  spectra:  $T_{pp} = 0.166$  GeV for the 2.76 TeV data and  $T_{pp} = 0.079$  GeV for the 5.02 TeV data, values that result from fitting to the  $pp$ -collisions data (see Supplementary Material for details). The dependencies of the parameters on the collision centrality, for both energies, are shown in Fig. 4.

The interplay between Lorentz transformations and drag effects establishes a relation between the original parton momentum  $p_T^o$  and the observed momentum  $p_T$ , as shown in Fig. A.5. In the left panel, the dynamics induce slight modifications to the momentum, resulting in an approximately linear relationship between  $p_T^o$  and  $p_T$ . The right panel displays the ratio  $p_T^o/p_T$  as a function of the logarithm of the observed momentum  $p_T$ , where dynamic effects become more evident. In this case, a log-periodic oscillation of the original momentum emerges, which gives rise to the oscillatory behaviour of  $R_{AA}$  and establishes a connection with the complex- $q$  approach, as discussed below.

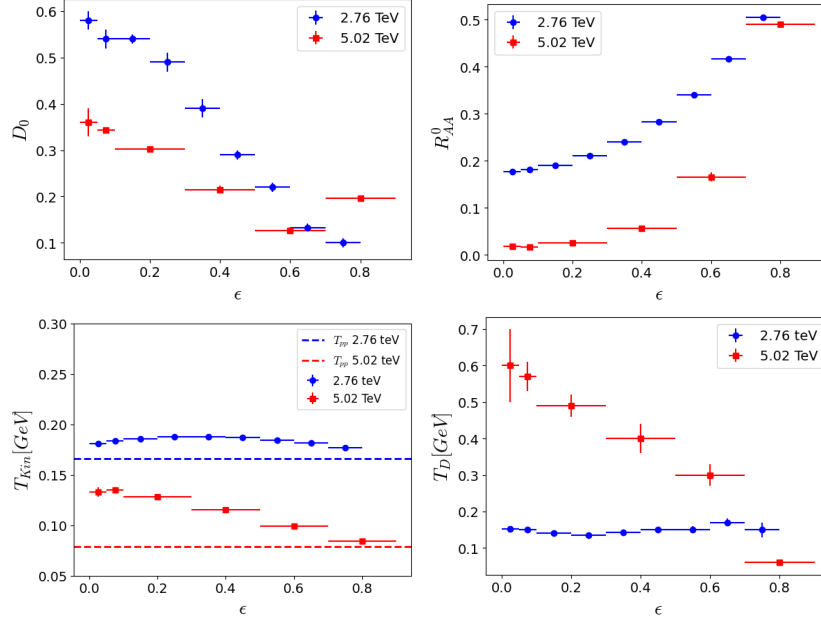


Figure 4: Fitted parameters as a function of centrality for  $\sqrt{s_{NN}} = 2.76$  TeV (blue) and  $\sqrt{s_{NN}} = 5.02$  TeV (red).

Figure 4 presents the best-fit values for additional model parameters. The parameter  $D_0$  (top-left) is associated with the phenomenological drift term, which depends on the particle momentum, as defined in Eqs. (14) and (28). The plots show an approximately linear decrease of  $D_0$  with the centrality parameter  $\epsilon$ , a trend observed at both collision energies. Since  $A_0$  is related to the drag effect and is primarily sensitive to the medium's properties rather than its geometry, it is reasonable to assume that  $A_0$  remains nearly constant with centrality. Thus, the linear behaviour reflects the variation of the interaction time  $\tau$  between the partons and the medium, from the multiparticle formation stage to freeze-out. This interaction time increases with centrality, reaching about 0.7 fm/c in the most central collisions, and tends toward zero in peripheral ones. This indicates that the medium in central collisions has a longer lifetime, consistent with the expectation that central collisions produce a more complex and long-lived system.

The top-right panel shows the parameter  $R_{AA}^0$ , which remains roughly constant in central collisions but exhibits a slight increase toward more peripheral ones. This trend can be attributed to geometric effects, particularly the ratio  $V_{AA}/V_{pp}$ , which becomes less reliably described by a linear dependence on centrality in more peripheral events. Although the trend is similar at both energies, the absolute values of  $R_{AA}^0$  differ significantly.

The bottom-left panel displays the temperature  $T_{AA}$  of the system formed in AA collisions, which is treated independently from the temperature in  $pp$  collisions. At 2.76 TeV, the temperature is nearly constant and slightly exceeds the  $pp$  value. At 5.02 TeV, however, a clear centrality dependence emerges. Since higher energies in-

volve larger parton momenta in the medium formation, this behavior may result from the neglect of relativistic effects in the PPE. Therefore, the observed centrality dependence likely stems more from approximations in the analytical treatment than from intrinsic physical properties of the medium's evolution.

The bottom-right panel presents the parameter  $T_D$ , which sets the energy scale in the phenomenological drag coefficient. At 2.76 TeV, it shows little dependence on centrality. At 5.02 TeV, larger uncertainties prevent a definitive conclusion, though the average value is slightly higher. Given the non-relativistic nature of the approximation, we refrain from assigning strong physical meaning to these results, including those for  $T_{Kin}$ . Nonetheless, the smooth behaviour of  $T_D$  supports the robustness of the phenomenological drag description and suggests it may serve as a reliable starting point for more realistic modelling.

The results indicate that the radial expansion velocity of the fluid is independent of collision centrality, with values of  $u = 0.99899c$  at 2.76 TeV and  $u = 0.9985c$  at 5.02 TeV, showing an almost negligible dependence on both centrality and collision energy. These values are significantly higher than those predicted by hydrodynamical models, which typically yield fluid velocities between 50% and 80% of the speed of light. However, it is important to note that in the blast-wave approach, the fluid velocity is constrained to be above the speed of sound, which can reach up to  $c_s \cong 0.6$  for the QGP [21, 22], whereas hydrodynamical models constrain the fluid velocity to remain below the speed of sound. Moreover, simplification adopted in the present calculations, such as the narrow cylindrical shell that contains the fluid in the freeze-out mechanism, can lead to enhanced velocity because of the higher energy density involved in the expansion.

In addition to the differing physical constraints intrinsic to the blast-wave and hydrodynamical approaches, this work adopts several simplifications aimed at deriving analytical expressions that enable connections with the complex- $q$  formalism. The assumption of a freeze-out surface with the fluid concentrated in a narrow cylindrical shell enhances the energy density and artificially increases the fluid velocity. The further assumption of a constant fluid velocity, independent of the radial coordinate  $r$ , also contributes to this overestimation. These constraints can be lifted in future numerical implementations. Aside from these considerations, another central aspect is the assumption that the QGP is a pionic fluid, corresponding to a mass of the fluid quasi-particle equal to the pion mass. If this effective mass is  $m \cong 2.7$  GeV, the fluid velocity reduces to  $u = 0.8$ .

### 3.1. The log-periodic oscillation in the dynamical picture

The log-periodic oscillation of  $p_T^o/p_T$  opens the opportunity to link the dynamics effects with the log-periodic oscillation observed in [1, 2]. This section establishes a possible link between the complex- $q$  approach and the dynamical approach, aiming to express the real and imaginary parts of  $q$  in terms of the dynamical parameters.

The starting point is the transformation between  $p_T$  and  $p_T^o$ , given by Eq. (18).

Using the Lorentz transformation, that equation results in <sup>3</sup>

$$\frac{p_T^o}{p_T} = \frac{p_M}{p_T} \left( \frac{X}{v} + \sqrt{1 + X^2} \right), \quad \text{where} \quad X \equiv \gamma_v \gamma_{v_T} (v_T - v) \exp[A(\bar{p}_T)\tau], \quad (29)$$

with  $v = p_M/(p_M^2 + m^2)^{1/2}$ ,  $v_T = p_T/m_T$  and  $\gamma_r = (1 - r^2)^{-1/2}$  for  $r = v, v_T$ .

The results obtained in the previous sections show that the ratio  $p_T^o/p_T$  remains close to unity in the relevant range of  $p_T$ . A Taylor expansion around  $A(\bar{p}_T)\tau = 0$  leads to

$$\frac{p_T^o}{p_T} \simeq 1 + \frac{p_T^2 - p_M^2}{p_T^2 + p_M^2} A(\bar{p}_T)\tau \simeq 1 + A_0\tau \frac{(p_T^2 - p_M^2)}{p_T^2 + p_M^2} \exp_q \left[ \frac{a}{T} - \frac{(p_T^2 + p_M^2)m}{2p_T p_M T} \right], \quad (30)$$

where in the second equality we have considered an expansion of  $A(\bar{p}_T)$  at small  $m$ . In this equation  $a$  is a constant that in the following we will set to zero for simplicity. Defining the variable  $y \equiv \bar{m}_T/m$  and performing a Taylor expansion around  $y = 1$ , which corresponds to  $\bar{p}_T = 0$ , Eq. (30) results in

$$\frac{p_T^o}{p_T} \simeq 1 + 2A_0\tau m (y - 1) \exp_q[-ym/T]. \quad (31)$$

Using now that  $\sin(y - 1) \simeq y - 1 \simeq \sin(\log y)$ , one arrives at the following result

$$\frac{p_T^o}{p_T} \simeq 1 + 2\tilde{A}_0\tau (1 + z)^{-m_0} \cos[c \log(1 + z)], \quad (32)$$

where

$$1 + z = e^{-\frac{\pi}{2c}} \frac{1 + x}{1 + x_o}, \quad y = x/x_o, \quad x_o = (q - 1)m/T, \quad c = 1 + 1/x_o, \quad (33)$$

while  $\tilde{A}_0 = \left( e^{\frac{\pi}{2c}} (1 + x_o) \right)^{\frac{1}{1-q}} m A_0$  and  $m_0 = 1/(q - 1)$ . This corresponds to a complex- $q$  Tsallis distribution of the form

$$\frac{p_T^o}{p_T} - 1 \simeq (1 + z)^{-\text{Re}(m_k)} \sum_{k=0}^{\infty} w_k \cos[\text{Im}(m_k) \log(1 + z)], \quad (34)$$

with

$$m_k = \frac{1}{q - 1} + ik \left( 1 + \frac{1}{x_o} \right), \quad (k = 0, 1, 2, \dots). \quad (35)$$

Only the term  $k = 1$  is present in Eq. (34), i.e.  $w_1 = 2\tilde{A}_0\tau \neq 0$  and  $w_n = 0 \forall n \neq 1$ . In an expansion around  $q = 1$ , one has

$$q_k = 1 + \frac{1}{m_k} \simeq 1 + \frac{1 - i\xi_k}{1 + \xi_k^2} (q - 1) + O((q - 1)^2), \quad (36)$$

where  $\xi_k \equiv kT/(2m)$ . Notice that  $q_k \rightarrow q$  for  $T/m \rightarrow 0$  when  $q$  is close to 1.

---

<sup>3</sup>In Eq. (29),  $v$  and  $v_T$  denote the components of the 3-vectors in the transverse direction.

#### 4. Conclusions and outlook

In summary, this work calculates the nuclear suppression factor of charged particles in Pb–Pb collisions at two collision energies: 2.76 TeV and 5.02 TeV. The novel approach incorporates dynamical effects within the framework of the Plastino–Plastino Equation, considering a  $q$ -exponential ansatz for the drag coefficient, which leads to momentum depletion. The effect of diffusion is found to be negligible in our calculations.

The results indicate that the oscillations observed in the  $R_{AA}$  data have a dynamical origin, stemming from the ratio between the initial and depleted momenta in the center-of-mass frame. This oscillatory behavior gives rise to a complex  $q$ -parameter. The theoretical model shows good agreement with experimental data at  $\sqrt{s} = 2.76$  TeV across all centralities and momentum ranges. Minor deviations in the high-momentum region can be attributed to simplifications introduced to obtain analytical expressions for the dynamical effects.

The satisfactory agreement between the model and the data underscores the relevance of log-periodic oscillations, which have been observed in other analyses as well. The connection established between the complex- $q$  formalism and the dynamical approach provides a new interpretation of complex- $q$  parameters, complementing existing interpretations.

This work can be extended to improve accuracy by allowing for numerical solutions of the fully relativistic Plastino–Plastino Equation. Such an approach would enhance our understanding of the role played by the drag transport coefficient in parton dynamics within the medium.

#### Acknowledgements

In preparation for this publication, we used the resources of the Centre for Computation and Computer Modelling of the Faculty of Exact and Natural Sciences of the Jan Kochanowski University in Kielce, modernised from the funds of the Polish Ministry of Science and Higher Education in the “Regional Excellence Initiative” programme under the project RID/SP/00015/2024/01. G. Wilk was supported in part by the Polish Ministry of Education and Science, Grant No. 2022/WK/01. R. Baptista’s work was supported by the project RID/SP/00015/2024/01. T. Bhattacharyya acknowledges funding from the European Union’s HORIZON EUROPE programme, via the ERA Fellowship Grant Agreement number 101130816. A D is partially supported by the CNPq, grant 306093/2022-7, and by FAPESP grant 24/01533-7. E M is supported by the Junta de Andalucía under grant FQM-225.

## Appendix A. Fittings of $pp$ collisions

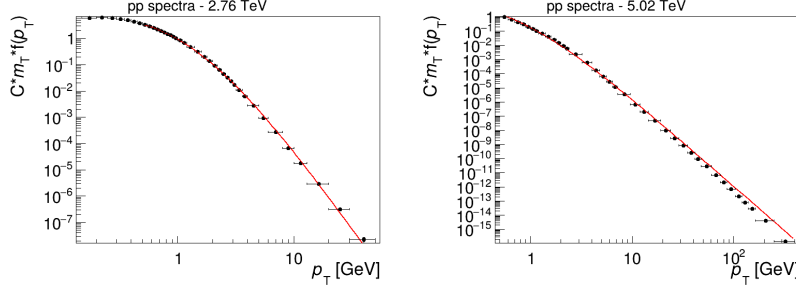


Figure A.5: Fittings of the transverse momentum spectra for  $pp$  data for 2.76 GeV (left) and 5.02 GeV (right) collision energies.  $C$  is a fitting constant,  $m_T$  the transverse mass and  $f(p_T)$  the momentum distribution function.

## Appendix B. Connection with wounded nucleon model

The collision energy is proportional to the number of participant nucleons,  $N_{\text{part}}$ . We have checked using the Glauber model-based GLISSANDO Monte-Carlo code [23] for the Pb-Pb collisions at 2.76 TeV that the number of participant nucleons can be written as,

$$N_{\text{part}} = 5.9 + 402 [1 - \epsilon]^{2.71}, \quad (\text{B.1})$$

where  $\epsilon$  is the centrality. Thus, the collision energy can be expressed as  $E \propto N_{\text{part}}$ , leading to

$$\frac{N}{E} \propto [5.9 + 402 [1 - \epsilon]^{2.71}]^{-d}. \quad (\text{B.2})$$

Using the same numerical framework, we also find that  $N_{\text{coll}} \approx 0.35 [N_{\text{part}}]^{1.4}$ .

## Appendix C. Inclusion of the diffusive effects

The effects of the diffusion on the transverse momentum distribution are characterized by the broadening of the  $p_T$  distribution as the parton travels through the medium. The width of the distribution is given by [24]

$$\sigma(t) = \sigma_o [(1 - \kappa) \exp(-\xi A t) + \kappa]^{1/\xi}, \quad (\text{C.1})$$

where  $\sigma_o$  is the initial distribution width,  $\kappa$  is a constant that depends on the transport coefficients  $A$  and  $D$ , and  $\xi = 5 - 3q$ .

The effects of the inclusion of the diffusion effects in  $R_{AA}(p_T)$  were included by considering that the original transverse momentum of the parton, before its interaction with the medium, not given by Eq. (18) anymore, but by a set of value  $p_m$  which,

after the dynamics effects, will end up being  $p_T$  with some probability given by the  $q$ -gaussian probability distribution

$$G_q(p_m, p) = e_q \left( -\frac{(p - p_m)^2}{2\pi\sigma(\tau)^2} \right), \quad (\text{C.2})$$

The nuclear-nuclear distribution becomes.

$$f_D^{AA}(p_T) = \mathcal{N} \int G_q(L_u[p_m], L_u[p_T]) f(L_{-u}[L_u[p_m] \exp(A\tau)]) dp_o, \quad (\text{C.3})$$

with

$$\mathcal{N}^{-1} = \int G_q(L_u[p_m], L_u[p_T]) dp_o. \quad (\text{C.4})$$

where  $\mathcal{N}$  is a normalization constant.

#### Appendix C.1. Dynamical effects on the original and observed momenta

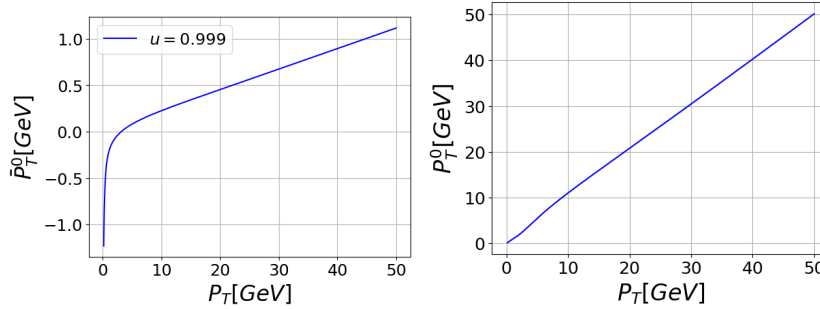


Figure C.6: (Left) The initial parton momentum in the local rest frame of the fluid. (Right) The momentum of the parton in the moment it was created,  $p_T^o$ , as a function of the observed momentum  $p_T$ .

#### Appendix D. Alternative connection with complex- $q$ formalism

A formula that constitutes a good approximation for  $p_T^o/p_T$  is

$$\frac{p_T^o}{p_T} \cong 1 + \left(1 + \frac{p_T}{p_M}\right)^{-m_o} [w_0 + w_1 \cos[c \log(1 + p_T/p_M)] + w_2 \cos[2c \log(1 + p_T/p_M)]], \quad (\text{D.1})$$

where

$$m_o = -\frac{\ln(1 - \alpha n)}{\ln(1 + \alpha)}, \quad c = \frac{2\pi}{\ln(1 + \alpha)}, \quad (\text{D.2})$$

and

$$\alpha = 22.14, \quad n = 0.04515, \quad w_0 = \frac{1}{2}, \quad w_1 = -1, \quad w_2 = \frac{1}{2}. \quad (\text{D.3})$$

The real part of the associated  $\hat{q}$  parameter is

$$\text{Re}(\hat{q}) \simeq 1 + \frac{1}{m_0} \simeq 1.41 \quad (k = 0). \quad (\text{D.4})$$

The results of Eq. (D.1) compared with the previous results are displayed in Fig. D.7 (left).

It is possible to find an explicit log-oscillatory expression by considering the following steps. Let us define the variable  $y \equiv \frac{(p_T^2 + p_M^2)}{2p_T p_M}$ . Then, the factor multiplying the  $q$ -exp function in Eq. (30) writes, in terms of it as

$$\frac{p_T^2 - p_M^2}{p_T^2 + p_M^2} \simeq \pm \sqrt{2(y-1)}, \quad (\text{D.5})$$

where we have considered a Taylor expansion around  $y = 1$ . Using now that  $y - 1 \simeq \ln(y - 1)$  and  $y - 1 \simeq \ln(y)$ , we find the following result

$$\left( \frac{p_T^o}{p_T} - 1 \right)^2 \cong 2(A_0 \tau)^2 \exp_q \left[ -\frac{2(my-a)}{T} \right] \cos \left[ \log(y) - \frac{\pi}{2} \right], \quad (\text{D.6})$$

where we have approximated also  $(\exp_q[x])^2 \simeq \exp_q[2x]$ . This result is displayed in Fig. D.7 (right).

On the other hand, by defining the new variable  $x$  as  $y \equiv x/x_o$  with  $x_o = 2(q-1)m/T$ , and after considering also an expansion around  $x = x_o$ , corresponding to  $y = 1$ , this result can be expressed in the form

$$\left( \frac{p_T^o}{p_T} - 1 \right)^2 \cong 2(A_0 \tau)^2 (1+x)^{-\frac{1}{q-1}} \cos \left[ \tilde{c} \log(1+x) + \tilde{f} \right], \quad (\text{D.7})$$

where

$$\tilde{c} = 1 + \frac{1}{x_o}, \quad \tilde{f} = -\frac{\pi}{2} - \tilde{c} \log(1+x_o). \quad (\text{D.8})$$

We have set  $a = 0$ . This corresponds roughly to a complex- $q$  Tsallis distribution with

$$m_k = \frac{1}{q-1} + ik \left( 1 + \frac{1}{x_o} \right), \quad (k = 0, 1, 2, \dots). \quad (\text{D.9})$$

The 'exact'  $q$ -complex Tsallis distribution is obtained by using the variable  $z$ , defined as

$$1+z = e^{-\frac{\pi}{2\tilde{c}}} \frac{1+x}{1+x_o}. \quad (\text{D.10})$$

In terms of this variable, Eq. (D.7) writes

$$\left( \frac{p_T^o}{p_T} - 1 \right)^2 \cong 2(\tilde{A}_0 \tau)^2 (1+z)^{-\frac{1}{q-1}} \cos [\tilde{c} \log(1+z)], \quad (\text{D.11})$$

where

$$\tilde{A}_0 \equiv \left( e^{\frac{\pi}{2\tilde{c}}} (1+x_o) \right)^{\frac{1}{2(1-q)}} A_0. \quad (\text{D.12})$$

The results for the complex  $q_k$  parameters are

$$q_k = 1 + \frac{1}{m_k} = 1 + \frac{\text{Re}(m_k)}{|m_k|^2} - i \frac{\text{Im}(m_k)}{|m_k|^2} = 1 + \frac{1}{|m_k|^2(q-1)} - ik \frac{1+1/x_o}{|m_k|^2}, \quad (\text{D.13})$$



with  $|m_k|^2 = 1/(q-1)^2 + [k(1+1/x_o)]^2$ . In an expansion around  $q = 1$ , one has

$$q_k \simeq 1 + \frac{1 - i\xi_k}{1 + \xi_k^2} (q-1) + O((q-1)^2), \quad (\text{D.14})$$

where  $\xi_k \equiv kT/(2m)$ . Notice that  $q_k \rightarrow q$  for  $T/m \rightarrow 0$  and  $q \rightarrow 1$ . The result is better if one doesn't consider the approximation  $(\exp_q[x])^2 \simeq \exp_q[2x]$ . In this case, one should define  $1+z = e^{-\frac{\pi}{\tilde{c}}} \left( \frac{1+x}{1+x_o} \right)^2$ . Then, one has

$$\left( \frac{p_T^o}{p_T} - 1 \right)^2 \simeq 2(\tilde{A}_0\tau)^2 (1+z)^{-\frac{1}{q-1}} \cos \left[ \frac{\tilde{c}}{2} \log(1+z) \right], \quad (\text{D.15})$$

with

$$m_k = \frac{1}{q-1} + i\frac{k}{2} \left( 1 + \frac{1}{x_o} \right), \quad \tilde{A}_0 \equiv \left( e^{\frac{\pi}{2\tilde{c}}} (1+x_o) \right)^{\frac{1}{(1-q)}} A_0, \quad x_o = (q-1)m/T, \quad \tilde{c} = 1+1/x_o. \quad (\text{D.16})$$

Eq. (D.14) holds also in this case. In summary, the  $q$ -complex Tsallis distribution can be obtained by considering the variable

$$z = e^{-\frac{\pi}{\tilde{c}}} \left( \frac{1+x}{1+x_o} \right)^2 - 1, \quad \text{where} \quad x = x_o \frac{p_T^2 + p_M^2}{2p_T p_M}, \quad x_o = (q-1)m/T, \quad \tilde{c} = 1+1/x_o. \quad (\text{D.17})$$

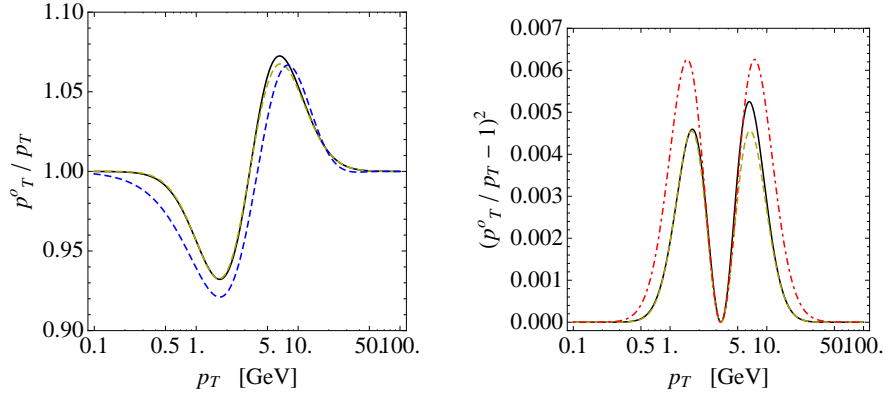


Figure D.7: (Left) Ratio  $p_T^o/p_T$  as a function of  $p_T$ . We display in dashed (blue) the approximation given by Eq. (31). (Right) Deviation  $(p_T^o/p_T - 1)^2$  as a function of  $p_T$ . We display in dotdashed (red) the approximation given by Eq. (D.6). The other lines in both panels are: solid (black) is the result of Eq. (29), and dashed (yellow) the result of Eq. (30).

## Appendix E. Log-oscillations in $R_{AA}$

Let us study how the log-oscillations in  $p_T^o/p_T$  produce log-oscillations in  $R_{AA}$ . The particle momentum distribution is

$$f^{AA}(p_T) = f(p_T^o) = \left[ 1 + (q-1) \frac{p_T^o}{\lambda} \right]^{-\frac{1}{q-1}} = \left[ 1 + (q-1) \frac{p_T}{\lambda} \frac{p_T^o}{p_T} \right]^{-\frac{1}{q-1}}. \quad (\text{E.1})$$

By using now that  $p_T^o/p_T \simeq 1 + Y(p_T)$  where  $Y(p_T)$  is a small oscillatory contribution, one can make a Taylor expansion of this expression up to order  $O(Y)$ , to get

$$f^{AA}(p_T) \simeq \left[1 + (q-1)\frac{p_T}{\lambda}\right]^{-\frac{1}{q-1}} \times \left[1 - \frac{p_T/\lambda}{1 + (q-1)p_T/\lambda} Y(p_T)\right]. \quad (\text{E.2})$$

Moreover

$$\begin{aligned} R_{AA}(p_T) &= [N_{AA}(1-\epsilon)]^{-d} \frac{V_{AA}}{V_{pp}} \frac{f^{AA}(p_T)}{f(p_T)} \\ &\simeq [N_{AA}(1-\epsilon)]^{-d} \frac{V_{AA}}{V_{pp}} \left[1 - \frac{p_T/\lambda}{1 + (q-1)p_T/\lambda} Y(p_T)\right]. \end{aligned} \quad (\text{E.3})$$

Then, the oscillations in  $Y(p_T)$  induce oscillations in  $f^{AA}(p_T)$  and  $R_{AA}(p_T)$ . The result for  $R_{AA}(p_T)$  is displayed in Fig. E.8.

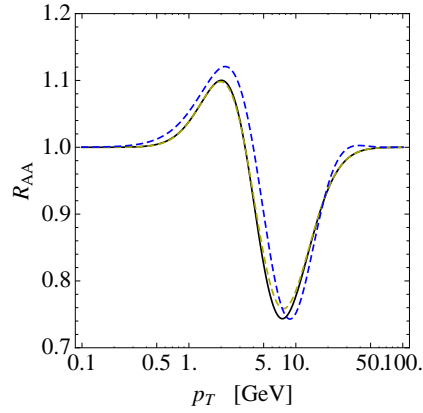


Figure E.8:  $R_{AA}$  as a function of  $p_T$  by using Eq. (E.3). We have considered  $\lambda = 1$  GeV.

Other way to arrive at this result is by using

$$\left[1 + (q-1)\frac{p_T^o}{\lambda}\right]^{-\frac{1}{q-1}} \cong \left[1 + (q-1)\frac{p_T}{\lambda}\right]^{-\frac{1}{q-1}} \left(\frac{p_T^o}{p_T}\right)^{-\frac{1}{q-1}}, \quad (\text{E.4})$$

which is valid for  $p_T, p_T^o \gg \lambda$ . Then

$$R_{AA}(p_T) \simeq [N_{AA}(1-\epsilon)]^{-d} \frac{V_{AA}}{V_{pp}} \left(\frac{p_T^o}{p_T}\right)^{-\frac{1}{q-1}} \simeq [N_{AA}(1-\epsilon)]^{-d} \frac{V_{AA}}{V_{pp}} \left(1 - \frac{1}{q-1} Y(p_T)\right). \quad (\text{E.5})$$

This result is in agreement with Eq. (E.3) for  $p_T \gg \lambda$ , but not for  $p_T \lesssim \lambda$ . According to the experimental data for  $R_{AA}(p_T)$ , the corrections are of order  $Y(p_T) \sim 10\%$  and

$\frac{1}{q-1}Y(p_T) \sim 65\%$ . Finally, an expression for  $R_{AA}(p_T)$  valid even if  $Y(p_T)$  is not small is

$$\begin{aligned} R_{AA}(p_T) &\simeq [N_{AA}(1-\epsilon)]^{-d} \frac{V_{AA}}{V_{pp}} \left( \frac{p_T^o}{p_T} \right)^{-\frac{1}{q-1}} = [N_{AA}(1-\epsilon)]^{-d} \frac{V_{AA}}{V_{pp}} \left( 1 + \frac{q-1}{q-1} Y(p_T) \right)^{-\frac{1}{q-1}} \\ &= [N_{AA}(1-\epsilon)]^{-d} \frac{V_{AA}}{V_{pp}} \exp_q \left[ -\frac{1}{q-1} Y(p_T) \right]. \end{aligned} \quad (\text{E.6})$$

## References

- [1] G. Wilk and Z. Włodarczyk, “Tsallis distribution with complex nonextensivity parameter  $q$ ,” *Physica A: Statistical Mechanics and its Applications*, vol. 413, p. 53–58, 2014.
- [2] M. Rybczyński, G. Wilk, and Z. Włodarczyk, “System size dependence of the log-periodic oscillations of transverse momentum spectra,” *EPJ Web of Conferences*, vol. 90, p. 01002, 2015.
- [3] G. Wilk and Z. Włodarczyk, “Tsallis distribution decorated with log-periodic oscillation,” *Entropy*, vol. 17, p. 384–400, 2015.
- [4] G. Wilk and Z. Włodarczyk, “Sound waves in hadronic matter,” *EPJ Web Conf.*, vol. 172, p. 01002, 2018.
- [5] G. Wilk and Z. Włodarczyk, “Temperature oscillations and sound waves in hadronic matter,” *Physica A*, vol. 486, pp. 579–586, 2017.
- [6] Alice Collab., “Transverse momentum spectra and nuclear modification factors of charged particles in pp, p-Pb and Pb-Pb collisions at the LHC,” *Journal of High Energy Physics*, vol. 2018, p. 013, 2018.
- [7] CMS Collab., “Nuclear modification factor of  $D^0$  mesons in PbPb collisions at 5.02 TeV,” *Physics Letters B*, vol. 782, p. 474–496, July 2018.
- [8] E. Megías, A. Deppman, R. Pasechnik, and C. Tsallis, “Comparative study of the heavy-quark dynamics with the Fokker-Planck equation and the Plastino-Plastino equation,” *Physics Letters B*, vol. 845, p. 138136, 2023.
- [9] T. Bhattacharyya, “Nonextensive Boltzmann transport equation: The relaxation time approximation and beyond,” *Physica A: Statistical Mechanics and its Applications*, vol. 624, p. 128910, 2023.
- [10] T. Bhattacharyya, E. Megías, and A. Deppman, “Jet quenching of the heavy quarks in the quark-gluon plasma and the nonadditive statistics,” *Physics Letters B*, vol. 856, p. 138907, 2024.
- [11] F. Cooper and G. Frye, “Single-particle distribution in the hydrodynamic and statistical thermodynamic models of multiparticle production,” *Physical Review D*, vol. 10, no. 1, p. 186–189, 1974.

- [12] S. Grigoryan, “Using the Tsallis distribution for hadron spectra in pp collisions: Pions and quarkonia at 5gev,” *Physical Review D*, vol. 95, p. 056021, 2017.
- [13] D. B. Walton and J. Rafelski, “Equilibrium distribution of heavy quarks in Fokker-Planck dynamics,” *Phys. Rev. Lett.*, vol. 84, pp. 31–34, Jan 2000.
- [14] A. Plastino and A. Plastino, “Non-extensive statistical mechanics and generalized Fokker-Planck equation,” *Physica A: Statistical Mechanics and its Applications*, vol. 222, no. 1–4, p. 347–354, 1995.
- [15] G. Chacón-Acosta and G. M. Kremer, “Fokker-planck-type equations for a simple gas and for a semirelativistic Brownian motion from a relativistic kinetic theory,” *Physical Review E*, vol. 76, p. 02120, 2007.
- [16] L. Q. Rocha, E. Megías, L. A. Trevisan, K. K. Olimov, F. Liu, and A. Deppman, “Nonextensive statistics in high energy collisions,” *Physics*, vol. 4, no. 2, p. 659–671, 2022.
- [17] A. Deppman, E. Megías, and D. P. P. Menezes, “Fractal structures of Yang–Mills Fields and non-extensive statistics: Applications to high energy physics,” *Physics*, vol. 2, p. 455–480, 2020.
- [18] B. Abelev, J. Adam, D. Adamová, A. M. Adare, M. M. Aggarwal, G. A. Rinella, A. G. Agocs, A. Agostinelli, S. A. Salazar, Z. Ahammed, *et al.*, “Centrality dependence of charged particle production at large transverse momentum in Pb–Pb collisions at  $\sqrt{s_{NN}} = 2.76$  TeV,” *Physics Letters B*, vol. 720, no. 1–3, pp. 52–62, 2013.
- [19] V. Khachatryan *et al.*, “Charged-particle nuclear modification factors in PbPb and pPb collisions at  $\sqrt{s_{NN}} = 5.02$  TeV,” *JHEP*, vol. 04, p. 039, 2017.
- [20] A. Deppman, E. Megías, and D. P. Menezes, “Fractals, nonextensive statistics, and QCD,” *Physical Review D*, vol. 101, no. 3, p. 034019, 2020.
- [21] S. Borsányi, G. Endrődi, Z. Fodor, A. Jakovác, S. D. Katz, S. Krieg, C. Ratti, and K. K. Szabó, “The QCD equation of state with dynamical quarks,” *Journal of High Energy Physics*, vol. 2010, p. 077, 2010.
- [22] A. Bazavov, T. Bhattacharya, C. DeTar, H.-T. Ding, S. Gottlieb, R. Gupta, P. Hegde, U. Heller, F. Karsch, E. Laermann, L. Levkova, S. Mukherjee, P. Petreczky, C. Schmidt, C. Schroeder, R. Soltz, W. Soeldner, R. Sugar, M. Wagner, and P. Vranas, “Equation of state in 2+1 flavor QCD,” *Physical Review D*, vol. 90, p. 094503, 2014.
- [23] P. Božek, W. Broniowski, M. Rybczynski, and G. Stefanek, “GLISSANDO 3: GLauber Initial-State Simulation AND mOre..., ver. 3,” *Comput. Phys. Commun.*, vol. 245, p. 106850, 2019.
- [24] E. Megías, A. Khalili Golmankhaneh, and A. Deppman, “Dynamics in fractal spaces,” *Physics Letters B*, vol. 848, p. 138370, 2024.